Title

Regulation of the Rhp26ERCC6/CSB chromatin remodeler by a novel conserved leucine latch motif

Journal

Proceedings of the National Academy of Sciences of the United States of America, 111(52)

ISSN

0027-8424

Authors

Wang, Lanfeng
Limbo, Oliver
Fei, Jia
et al.

Publication Date

2014-12-30

DOI

10.1073/pnas.1420227112

Peer reviewed

Regulation of the Rhp26$^{ERCC6/CSB}$ chromatin remodeler by a novel conserved leucine latch motif

Lanfeng Wang[a,1], Oliver Limbo[b,1], Jia Fei[c], Lu Chen[d,e], Bong Kim[f], Jie Luo[f], Jenny Chong[a], Ronald C. Conaway[d,e], Joan W. Conaway[d,e], Jeff A. Ranish[f], James T. Kadonaga[c], Paul Russell[b], and Dong Wang[a,2]

[a]Skaggs School of Pharmacy and Pharmaceutical Sciences, University of California, San Diego, La Jolla, CA 92093; [b]Department of Cell and Molecular Biology, The Scripps Research Institute, La Jolla, CA 92037; [c]Section of Molecular Biology, University of California, San Diego, La Jolla, CA 92093; [d]Stowers Institute for Medical Research, Kansas City, MO 64110; [e]Department of Biochemistry and Molecular Biology, Kansas University Medical Center, Kansas City, KS 66160; and [f]Institute for Systems Biology, Seattle, WA 98109

Edited by Philip C. Hanawalt, Stanford University, Stanford, CA, and approved November 26, 2014 (received for review October 22, 2014)

CSB/ERCC6 (Cockayne syndrome B protein/excision repair cross-complementation group 6), a member of a subfamily of SWI2/SNF2 (SWItch/sucrose nonfermentable)-related chromatin remodelers, plays crucial roles in gene expression and the maintenance of genome integrity. Here, we report the mechanism of the autoregulation of Rhp26, which is the homolog of CSB/ERCC6 in *Schizosaccharomyces pombe*. We identified a novel conserved protein motif, termed the "leucine latch," at the N terminus of Rhp26. The leucine latch motif mediates the autoinhibition of the ATPase and chromatin-remodeling activities of Rhp26 via its interaction with the core ATPase domain. Moreover, we found that the C terminus of the protein counteracts this autoinhibition and that both the N- and C-terminal regions of Rhp26 are needed for its proper function in DNA repair in vivo. The presence of the leucine latch motif in organisms ranging from yeast to humans suggests a conserved mechanism for the autoregulation of CSB/ERCC6 despite the otherwise highly divergent nature of the N- and C-terminal regions.

chromatin remodeling | SWI2/SNF2 | SNF2-like family ATPase | enzyme autoregulation | flanking regions

SWI2/SNF2 (switch/sucrose nonfermentable) and related ATP-dependent chromatin-remodeling enzymes in the SNF2-like family of proteins play essential roles in many aspects of DNA metabolism, including replication, transcription, recombination, and repair (1). These SNF2-like ATPases are broadly conserved throughout evolution and share a common core ATPase domain. Whereas the core motor ATPase domain provides the driving force for DNA translocation and chromatin-remodeling activity, emerging evidence suggests important roles of the flanking regions in mediating specific interactions with nucleosomes or other protein factors, substrate specificity, and the regulation of the function of the motor (2–7).

Cockayne syndrome group B protein (CSB/ERCC6) belongs to a subfamily of the SNF2-like family of ATPases (8) that plays a crucial role in transcription elongation and transcription-coupled repair (TCR), a specialized repair pathway that repairs DNA lesions in the transcribed genome (9–17). CSB is involved in the initiation steps of TCR in a manner that depends upon its chromatin remodeling and ATPase activities (18–21). Human CSB mutations are associated with Cockayne syndrome, a rare autosomal-recessive neurologic disorder characterized with progeriod features, growth failure, and photosensitivity (13, 21, 22).

CSB/ERCC6 proteins are conserved from yeast to humans (Fig. 1*A*). Particularly, the core ATPase domain is highly conserved not only within the ERCC6 subfamily (Fig. 1*A*) but also among other SNF2-like family members. The core ATPase domain is composed of two RecA-like domains (lobe 1 and lobe 2) and shares the hallmark signature of seven SF2 helicase motifs (motif I, Ia, II, III, IV, V, and VI). In addition to two conserved lobes, the core domain contains two α-helical domain insertions (HD1 and HD2) that are present in other SNF2-like family proteins such as Rad54 (23, 24). We therefore used the structure of Rad54 as a model for the CSB core ATPase domain. As shown in Fig. 1*B* (PDB ID code 1Z3I) (23), lobe 1 (blue) and lobe 2 (red) are connected by a hinge region (yellow), which is flexible and allows rotation between the two lobes during each cycle of ATP hydrolysis and DNA translocation (23, 24).

In sharp contrast, the N- and C-terminal flanking regions are not well conserved, and the length of these flanking regions varies significantly across species. Among the six representative CSB proteins shown in Fig. 1*A*, human CSB has the longest flanking regions whereas the shortest flanking regions are found in the *Schizosaccharomyces pombe* CSB homolog, Rhp26. Moreover, two previously identified domains in human CSB flanking regions, the acidic-rich region (356–394) and the ubiquitin binding domain (1400–1428) (13, 25, 26), are absent in Rhp26. Recent studies have suggested that the flanking regions of human CSB play regulatory roles in its enzymatic activities (20, 27). However, the molecular mechanisms underlying these regulatory activities by flanking regions are poorly understood. Moreover, the highly divergent nature of these flanking regions also raises the question whether there is a conserved mechanism by these regions regulating CSB activity.

To address the mechanism of autoregulation of CSB proteins, we focused on Rhp26, one of the shortest CSB homologs, as the model protein. We identified a novel conserved motif in the N-terminal region, which we term the "leucine latch" motif, that interacts with lobe 2 of the core ATPase domain and hinge region. This specific protein–protein interaction restricts the rotation of

Significance

Cockayne syndrome group B protein/excision repair cross-complementation group 6 (CSB/ERCC6) belongs to a subfamily of SWI2/SNF2 (SWItch/sucrose nonfermentable)-related chromatin-remodeling complexes. Defects in the CSB protein result in Cockayne syndrome, which is a rare autosomal-recessive neurologic disorder clinically characterized with progeriod features, growth failure, and photosensitivity. However, it remains poorly understood how the CSB enzymatic activity is regulated for CSB to perform its desired biological functions. Here, we reveal the molecular mechanism of autoinhibition of CSB enzymatic activities. We identify a novel conserved motif (leucine latch motif) that interacts with lobe 2 of the core ATPase domain and hinge region and locks the enzyme into an inactive conformation as a latch. This work provides important novel mechanistic insights into the autoregulation of CSB/ERCC6 proteins.

Author contributions: L.W., O.L., R.C.C., J.W.C., J.A.R., J.T.K., P.R., and D.W. designed research; L.W., O.L., J.F., L.C., B.K., J.L., J.C., and D.W. performed research; L.W., O.L., J.F., L.C., B.K., J.L., J.C., R.C.C., J.W.C., J.A.R., J.T.K., P.R., and D.W. analyzed data; and L.W., O.L., J.F., L.C., J.C., R.C.C., J.W.C., J.A.R., J.T.K., P.R., and D.W. wrote the paper.

The authors declare no conflict of interest.

This article is a PNAS Direct Submission.

[1]L.W. and O.L. contributed equally to this work.

[2]To whom correspondence should be addressed. Email: dongwang@ucsd.edu.

This article contains supporting information online at www.pnas.org/lookup/suppl/doi:10.1073/pnas.1420227112/-/DCSupplemental.

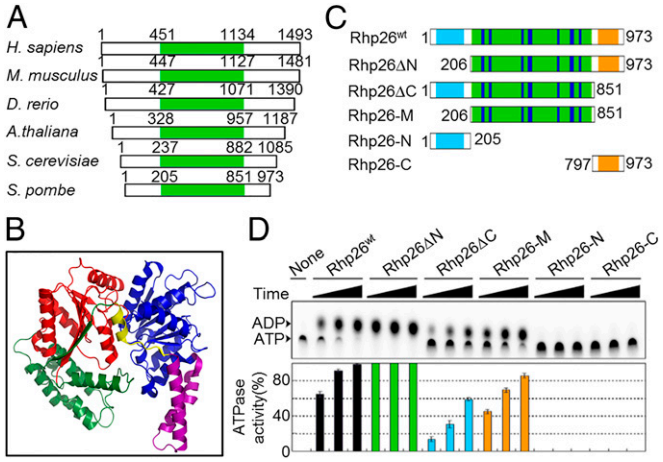

Fig. 1. CSB/ERCC6 contains a highly conserved ATPase core domain and divergent flanking regions that modulate its ATPase activity. (*A*) The CSB core ATPase domain (green) is highly conserved across species from yeast to humans. (*B*) Structure of the core ATPase domain shared among SWI2/SNF2 family members. Lobe 1, HD1, hinge, lobe 2, and HD2 are shown in blue, magenta, yellow, red, and green, respectively (23). (*C*) *S. Pombe* Rhp26 truncation constructs. The core ATPase domain is shown in green with seven conserved helicase motifs highlighted in blue. N- and C-terminal regions are shown in cyan and orange, respectively. (*D*) DNA-dependent ATPase activity of Rhp26 and Rhp26 truncations. Both the protein and DNA concentrations were at 500 nM. The reactions were performed at 30 °C for 15, 30, and 60 min, respectively. The error bars are the SD based on three independent experiments.

two lobes during translocation and inhibits the ATPase and chromatin-remodeling activities. The alteration of the leucine latch motif abolishes the autoinhibition of the ATPase and chromatin-remodeling activities and results in a hyperactive Rhp26 protein. Moreover, the strict conservation of this motif across species reveals an evolutionarily conserved regulatory mechanism in the ERCC6/CSB subfamily despite the highly divergent nature of flanking regions. Finally, we found that the C-terminal domain antagonizes the inhibition by the leucine latch and further showed that proper regulation by both the N- and C-terminal regions is important for cell survival and DNA damage repair. Taken together, we propose a new working model for a bifunctional autoregulatory mechanism of Rhp26/CSB activities.

Results

The ATPase Activity of Rhp26 Is Inhibited by Its N Terminus but Stimulated by Its C Terminus. To characterize the biochemical activity of Rhp26, we first compared the DNA-dependent ATPase activities of purified full-length recombinant Rhp26 protein ($Rhp26^{wt}$, 1–973) as well as five truncation mutant proteins, Rhp26ΔN(206–973), Rhp26ΔC(1–851), Rhp26-M(206–851), Rhp26-N(1–205), and Rhp26-C(797–973) (Fig. 1*C* and Fig. S1). Strikingly, the N-terminal region played a strong inhibitory role in regulating the ATPase activity of Rhp26 (comparison between pair of $Rhp26^{wt}$ vs. Rhp26ΔN, or Rhp26ΔC vs. Rhp26-M) whereas the C-terminal region played a positive regulatory role (comparison between pair of $Rhp26^{wt}$ vs. Rhp26ΔC, or Rhp26ΔN vs. Rhp26-M) (Fig. 1*D*). Rhp26ΔN had the highest ATPase activity whereas Rhp26ΔC showed the lowest ATPase activity among all of the Rhp26 proteins containing core ATPase domain (Fig. 1*D*). Intriguingly, like CSB, the N-terminal region (Rhp26-N) can also inhibit the ATPase activity of core domain (Rhp26-M) *in trans* (Fig. S2), suggesting that Rhp26-N is functionally conserved to the N-terminal region of CSB (CSB-N) despite the highly divergent nature of these flanking regions (20). As negative controls, Rhp26-N, Rhp26-C, and the "ATPase-dead" mutant Rhp26ΔNK308R (predicated by the sequence alignment with CSB) showed no ATPase activity (Fig. 1*D* and Fig. S3).

Deletion of N Terminus Greatly Stimulates Rhp26 Chromatin-Remodeling Activity. We examined the impact of flanking regions on the chromatin-remodeling activity of Rhp26 via two chromatin-remodeling assays using either purified mononucleosomes or chromatin as circular minichromosomes. Both assays revealed that only Rhp26ΔN has a robust ATP-dependent chromatin-remodeling activity among all of the Rhp26 variants we tested (Fig. 2). Intriguingly, Rhp26ΔN can even displace the histones to form a strong naked DNA band in an ATP-dependent manner in the mononucleosome-remodeling assay. No free DNA band was observed in the absence of ATP or in the presence of slow-hydrolysable ATPγS (lanes for protein 2 in Fig. 2*A*). As a negative control, no remodeling activity was observed for the ATPase-dead mutant, Rhp26ΔN-K308R (lanes for protein 3 in Fig. 2*A*). Full-length $Rhp26^{wt}$ failed to show strong chromatin-remodeling activity under the same experimental conditions, suggesting that it is in an autorepressed state by the N-terminal region. INO80 was used as a positive control, which remodels the mononucleosomes toward the centered positions of the DNA region, resulting in a slow-migrating band (lanes for protein 10 in Fig. 2*A*). We further tested the chromatin-remodeling activity by using the restriction enzyme accessibility assay with chromatin reconstituted onto circular plasmid DNA. ACF was used as a positive control. Consistent with the results from the mononucleosome-remodeling assay, only Rhp26ΔN showed strong chromatin-remodeling activity whereas no obvious chromatin-remodeling activity was observed for full-length Rhp26, Rhp26ΔN-K308R, and all other truncations (Fig. 2*B*). Taken together, these results indicate that deletion of the N-terminal region greatly enhances Rhp26 chromatin-remodeling activity.

In sharp contrast, Rhp26ΔC has no chromatin-remodeling activity but forms supershifted complexes with nucleosomes even in the presence of excess competing nucleosome and DNA (lanes for protein 4 in Fig. 2*A*). The formation of supershifted complexes depends upon the presence of ATP or ATPγS. Interestingly, the bands attributed to the supershifted complexes seemed stronger in the presence of ATP than that of

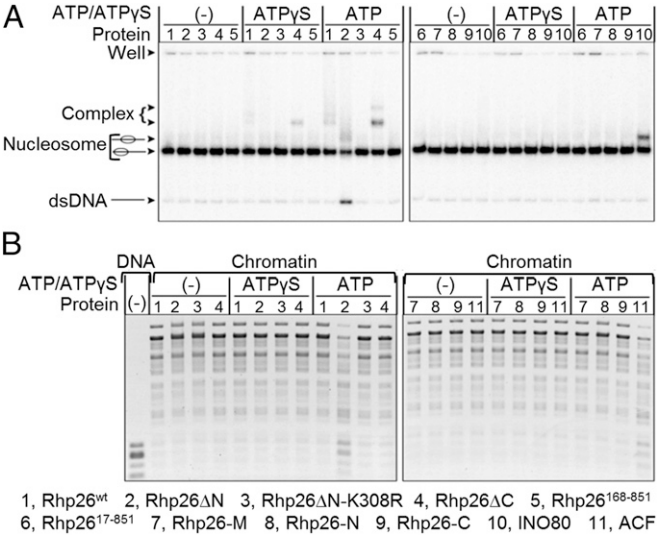

Fig. 2. Deletion of the N-terminal region greatly enhances the chromatin-remodeling activity of Rhp26. (*A*) Chromatin-remodeling assay with mononucleosome. Rhp26ΔN showed strong nucleosome-remodeling activity in the presence of ATP whereas no nucleosome-remodeling activity was observed for $Rhp26^{wt}$ and other truncations. Both $Rhp26^{wt}$ and Rhp26ΔC can bind the nucleosome to form a supercomplex in the presence of 1 mM ATP or ATPγS. (*B*) Chromatin-remodeling assay using a circular plasmid. Rhp26ΔN reveals strong remodeling activity in the presence of 3 mM ATP (lower bands). No chromatin-remodeling activity was observed for $Rhp26^{wt}$ and other truncations. The Rhp26 mutants are depicted in Fig. 1 and Fig. S5.

BIOCHEMISTRY

slow-hydrolysable ATPγS. This difference may indicate that the association of Rhp26 with nucleosome is dependent on both ATP binding and hydrolysis. This tight nucleosome binding of Rhp26ΔC relies on an intact N-terminal region because truncations of the N-terminal region abolish the supershifted complex bands (lanes for protein 5–7 in Fig. 2*A*). Full-length Rhp26 forms much weaker supershifted complex bands, suggesting that the presence of the C-terminal region weakens the nucleosome binding (lanes for protein 1 in Fig. 2*A*). Because of Rhp26ΔC's high nucleosome binding activity and low ATPase activity, it represents an inactive "locked state" that is inefficient for DNA translocation and chromatin remodeling.

In summary, the in vitro enzymatic characterizations clearly revealed that the N-terminal and C-terminal regions have opposing roles in regulating Rhp26 enzymatic activities. The N-terminal region greatly inhibits ATPase and chromatin-remodeling activities whereas C-terminal region stimulates these activities.

Rhp26 Activity Is Tightly Regulated and Balanced in Vivo. To test the role of Rhp26 in DNA damage repair in vivo, we analyzed the DNA damage sensitivity of *S. pombe* Rhp26 mutants. Consistent with the literature (28, 29), *rhp26Δ* cells are more sensitive to UV irradiation than wild-type (wt) cells (Fig. 3*A*). This UV irradiation sensitivity is further enhanced by the deletion of *uve1* (*uvde*), which acts in a parallel UV-damaged DNA endonuclease-dependent excision repair (UVER) pathway (Fig. S4*A*). In addition to UV irradiation, *rhp26Δ* cells are also more sensitive to DNA alkylating agents such as methyl methanesulfonate (MMS) (Fig. 3*A*).

To test the effects of flanking regions on Rhp26 function, we generated mutants that express wt or mutant Rhp26 with an N-terminal 3xFLAG and integrated them at the endogenous locus under the native promoter for testing DNA damage sensitivity (Fig. 3*A*). The *FLAG-rhp26*$^+$ strain behaved similarly to untagged wt strains, indicating that the FLAG tag does not noticeably interfere with Rhp26 function. Interestingly, *FLAG-rhp26ΔN* behaved similarly to wild type in regards to DNA damage sensitivity (with the exception to the highest dose of MMS), suggesting that the autoinhibition of the N-terminal region might be released upon DNA damage in vivo. The other *FLAG-rhp26* variants were as sensitive to DNA-damaging agents as a full deletion of Rhp26 (*rhp26Δ* strain), including the ATPase-dead *FLAG-rhp26-K308R* mutation, suggesting that the ATPase activity of Rhp26 is required for cellular resistance to DNA damage in vivo.

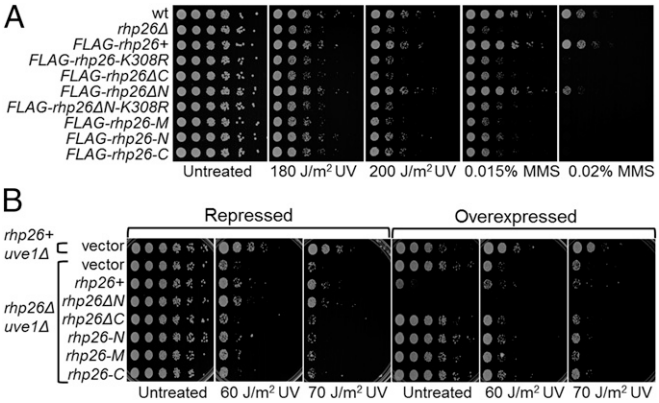

Fig. 3. Analysis of Rhp26 mutants in *S. pombe*. (*A*) DNA damage sensitivity assay for Rhp26 mutants. Rhp26 fragments were tagged with 3xFLAG epitope at the N terminus and inserted at the endogenous locus under the native promoter. (*B*) Overexpression of *rhp26*$^+$ and *rhp26ΔN* is toxic to *S. pombe*. *rhp26* constructs were under control of the thiamine repressible *nmt41* promoter and transformed into the indicated mutant background. Under repressed conditions, leaky expression partially rescues *rhp26Δ* in the case of wild-type and *rhp26ΔN* plasmids. Vector expressing 3xFLAG alone was used as a control. For all the above experiments, fivefold serial dilutions of log-phase cells with the indicated genotypes were plated and exposed to the indicated dose of UV irradiation or alkylating agent methyl methanesulfonate (MMS).

To further test the effects of flanking regions on Rhp26 function at different expression levels, we cloned the 3xFLAG-tagged constructs into plasmids under the control of the attenuated thiamine repressible *nmt41* promoter and transformed these plasmids into the *rhp26Δ uve1Δ* background (Fig. 3*B*). Similar to the result in Fig. 3*A* (at the endogenous locus under the native promoter), the very low level of expression of Rhp26 proteins in the presence of thiamine (repressed conditions) was sufficient for the *rhp26*$^+$ and *rhp26ΔN* constructs to partially complement *rhp26Δ uve1Δ* [Fig. 3*B*, *Left* (repressed)]. In sharp contrast, massive increases in protein expression levels of *rhp26*$^+$ and *rhp26ΔN* via derepression of the *nmt41* promoter (through the removal of thiamine) (Fig. S4*B*) surprisingly resulted in strong cellular toxicity even in the absence of UV irradiation (Fig. 3*B*, overexpressed, untreated condition). This cellular toxicity was greatly enhanced in the *rhp26ΔN* mutant, which failed to form visible colonies even under unchallenged conditions (Fig. 3*B*, overexpressed). These dominant-negative phenotypes of *rhp26*$^+$ and *rhp26ΔN* overexpression depend on their ATPase activities because the ATPase-dead K308R mutants abolish the cellular toxicity, suggesting that the toxicity was due to the unbalanced superactive ATPase activity of Rhp26 during overexpression (Fig. S4*C*). Over-expression of other less-active *rhp26* mutants did not cause cellular toxicity (Fig. 3*B*). Taken together, these results indicate that the in vivo Rhp26 activity is tightly regulated by its N- and C-terminal regulatory regions and protein expression to ensure efficient repair of DNA lesions while avoiding toxic effects arising from unbounded ATPase activity.

Identification of a Novel Motif That Plays an Important Regulatory Role. Because the N-terminal domain seemed to have an important role in regulating the enzymatic activities of Rhp26, we decided to closely examine and map the specific regions responsible for its regulatory roles by systematically comparing the enzymatic activities of a series of Rhp26ΔC variants with step-wise deletions of the N terminus. Intriguingly, we identified a short region (residues 6–16) at the N terminus that is important for the autoinhibition by the N-terminal region because deletion of this short region abolishes the N terminus's autoinhibition of Rhp26 ATPase activity (Fig. S5). The deletion of this region also abolishes the capability of Rhp26ΔC to form supershifted complexes with nucleosomes (Fig. 2*A*, lanes for protein 4 vs. lanes for protein 6).

Importantly, we found that this short region ((E/D)**L**xx**L**GVxx**Φ**x) is highly conserved from yeast to humans (Fig. 4*A*). We termed this novel motif as the leucine latch motif for its conserved Leu residues ($\mathbf{L}_7$xx$\mathbf{L}_{10}$) and functional roles. Secondary structure predictions indicate that part of this leucine latch motif (**L**xx**L**) likely forms a short helix, which is further connected with a downstream long stem helix to the rest of the N-terminal region (Fig. S6). We speculate that this short helix (**L**xx**L**) and hydrophobic Leu side chains may be important for locking Rhp26 in an "inactive locked state" as a latch. To test this idea, we mutated the corresponding leucine residues in Rhp26ΔC to glycine or proline, generating Rhp26ΔC-L7G/L10G and Rhp26ΔC-L7P/L10P, which are expected to remove hydrophobic side chains and disrupt the short helix. As shown in Fig. S5*C*, we observed a significant increase in the ATPase activity of Rhp26ΔC-L7G/L10G and Rhp26ΔC-L7P/L10P in comparison with Rhp26ΔC. Intriguingly, the ATPase activities of Rhp26ΔC-L7G/L10G and Rhp26ΔC-L7P/L10P are comparable with the ATPase activity of Rhp26-M, in which the entire N-terminal region is deleted (Fig. 1*D* and Fig. S5*C*).

We further tested the effect of the mutations of L7G/L10G and L7P/L10P on the full-length Rhp26 enzymatic activities (in the presence of the C-terminal region). Consistent with the results from Fig. S5*C*, Rhp26L7G/L10G and Rhp26L7P/L10P effectively rescued the inhibition of the N-terminal region on Rhp26 ATPase activity (Fig. 4*B*). More strikingly, Rhp26L7G/L10G and Rhp26L7P/L10P showed strong chromatin-remodeling activity and significantly rescued the inhibition of the N-terminal

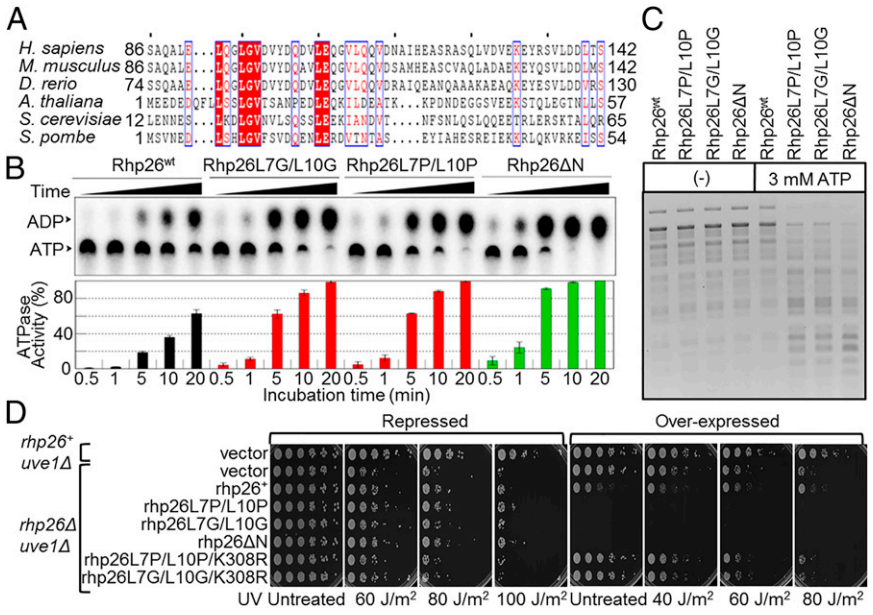

Fig. 4. The leucine latch motif is responsible for the autoregulation of Rhp26 activities by the N-terminal region. (*A*) A conserved leucine latch motif is revealed. Sequence alignment was generated using ClustalX (38) and the ESPript server (39). Conserved region, blue rectangle; strictly conserved residues, solid red. (*B*) Rhp26L7G/L10G and Rhp26L7P/L10P rescue the N-terminal region inhibition of Rhp26^{wt} ATPase activity. (*C*) Rhp26L7P/L10P or L7G/L10G mutations fully rescue the N-terminal region inhibition of chromatin-remodeling activity of Rhp26. The 200 ng of chromatin and 50 nM Rhp26 were used for each reaction. (*D*) Rhp26L7/L10 mutants have the same in vivo phenotypes as Rhp26ΔN. Fivefold serial dilutions of log-phase cells with the indicated genotypes were plated. The error bars in this figure are the SD based on three independent experiments.

region on Rhp26 chromatin-remodeling activity (Fig. 4*C*). Finally, we revealed that Rhp26L7G/L10G and Rhp26L7P/L10P mutants are functionally equivalent to the hyperactive mutant Rhp26ΔN in vivo (Fig. 4*D*).

Taken together, these experiments revealed that the L7G/L10G and L7P/L10P mutations recapitulate the effects of hyperactive Rhp26ΔN by abolishing the regulatory functions of the N-terminal region in modulating Rhp26 enzymatic activities in vitro (ATPase and chromatin-remodeling activities) as well as in vivo (cellular toxicity). Importantly, these results demonstrated that the leucine latch motif is required for the autoregulatory roles of the N-terminal region.

Mapping the Interaction of the N-Terminal Leucine Latch Motif with the Core ATPase Domain by Cross-Linking/Mass Spectrometry. To gain further mechanistic insights into how the leucine latch motif interacts with the core ATPase domain, we performed chemical cross-linking/mass spectrometry analysis to map their interactions using Rhp26ΔC. The cross-linker BS3 [Bis(sulfosuccinimidyl) suberate] allows us to cross-link the free amine group (-NH_2) at the N terminus (next to the leucine latch motif) with any nearby Lys ε–NH_2 residues of the core domain (the spacer length is 11.4 Å) (Fig. S7 *A–C*). These cross-links are highly specific, as we identified only 6 out of all of the possible 65 Lys residues in Rhp26ΔC (K132, K552, K560, K628, K742, and K817) that can form intramolecular cross-links with the short N-terminal peptide containing the leucine latch motif (Fig. 5*A* and Fig. S7*D*). Strikingly, we found that most of these specific cross-links are located in the highly conserved core ATPase domain, including the HD2 region (K552/K560) and lobe 2 (K628/K742) but not lobe 1 and the HD1 regions (Figs. 1*B* and 5*A*).

Further examination of the 3D distributions of these residues in the core ATPase domain based on a zebrafish Rad54 structure (Fig. 5*B*) (23) provided several important structural insights. First, these residues are located in a defined area within the same side of the core ATPase structure (cyan dashed circle in Fig. 5*B*, *Left*), suggesting a specific docking site for leucine latch motif at the N-terminal region (Fig. 5*B*, *Right*). Second, we noticed that two cross-link sites (K552 and K742) are very close to the hinge region connecting two lobes. It was proposed that during the translocation along the DNA, lobe 2 may rotate up to 180 degrees relative to lobe 1 from an open conformation to a closed conformation (24). K552 is located exactly at the region between the hinge region and lobe 2. K742 is also located close to the motif VI and highly conserved "Arg-finger residue" R734. Motif VI is proposed to mediate the interlobe communication, and residue R734 connects γ-phosphate of ATP. Thus, the interaction between the leucine latch motif and lobe 2 is likely to lock the relative movement of lobe 2 and lobe 1 during DNA translocation and chromatin remodeling. This result provides important structural insights into how the leucine latch motif at the N-terminal region inhibits the ATPase and chromatin-remodeling activity. Third, the other two cross-link sites (K560 and K628) are located at the interface between the HD2 region and lobe 2. HD2 is conserved among SWI2/SNF2 family and proposed to be involved in DNA binding. The interaction between the leucine latch motif and the HD2 region likely stabilizes the structure of lobe 2 and HD2 conformation and enhances nucleosomal DNA binding affinity.

Discussion

Mechanistic Insights into the Regulatory Role of a Novel Leucine Latch Motif in CSB Activities. Here, we reveal a novel molecular mechanism of how Rhp26$^{ERCC6/CSB}$ is regulated by flanking regions through a combination of biochemical, biophysical, and genetic approaches. We identified a new conserved leucine latch motif (residues 6–16, (E/D)**L**xx**L**GVxx**Φ**x) that functions as a latch to lock Rhp26 in a repressed state with low ATPase and chromatin-remodeling activities. This short motif is responsible for the regulatory role of the N-terminal region through specific interaction with lobe 2 and the HD2 region. Based on sequence analysis and secondary structure prediction, we anticipated that part of this motif (**L**xx**L**) forms a short helix that is important for regulation (Fig. 5*B* and Fig. S6). Indeed, double mutants Rhp26L7G/L10G and Rhp26L7P/L10P that disrupt this short helix can fully abolish the inhibitory effect of the N-terminal region and function equivalently to Rhp26ΔN both in vitro and in vivo. However, it should be noted that the complete motif may extend through the entire conserved region, such as the segment that corresponds to residues 6–28 of Rhp26 (Fig. 4*A*). Intriguingly, the leucine latch motif is highly conserved among the CSB homologs across species despite the generally low conservation in the N-terminal region, suggesting that this leucine latch motif-mediated regulation is likely to be an evolutionarily conserved mechanism.

Importantly, our study reveals novel mechanistic insights into ERCC6 subfamily enzymatic regulation through the leucine latch motif at the N-terminal region. The opening and closing of the interlobe cleft and relative rotation between lobe 1 and lobe 2 during the ATP hydrolysis cycle is proposed to cause the

BIOCHEMISTRY

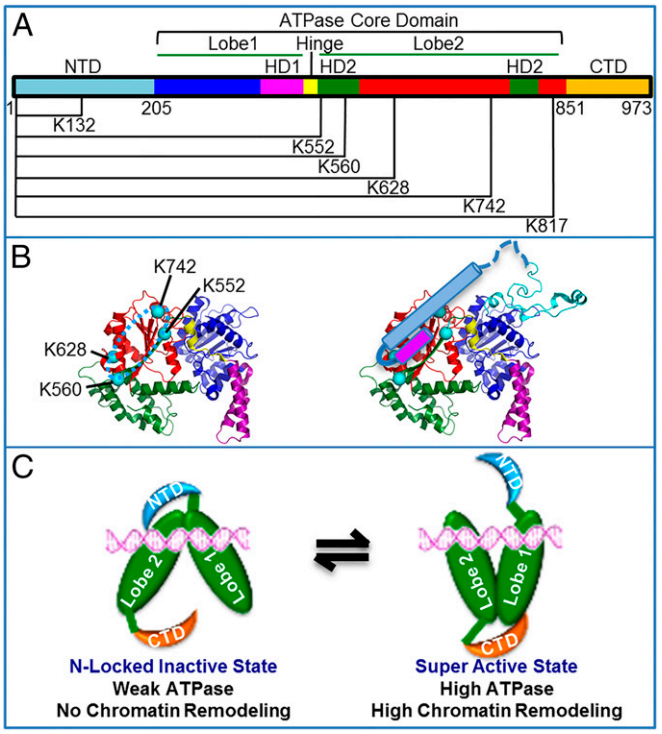

Fig. 5. Novel regulatory mechanism of Rhp26 by the flanking regions. (*A*) Specific cross-linking between the Rhp26 N terminus and the core ATPase domain. The different motifs were defined based on the sequence alignment of Rhp26 with zebrafish Rad54 (PDB ID code 1Z3I). The N-terminal region, lobe1, HD1, hinge, HD2, lobe 2, and the C-terminal region are shown in cyan, blue, magenta, yellow, green, red, and orange, respectively. The specific intramolecular cross-links between the N terminus and corresponding residues are depicted. (*B*) The docking site for the Rhp26 N terminus based on the above cross-linking data is shown as a dashed cyan oval (*Left*) and locking model of the Rhp26 N-terminal region (leucine latch motif). Four Lys residues from HD2 and lobe 2 identified from the cross-linking study are highlighted in cyan spheres. The conserved leucine latch motif [magenta helix (cylinder), *Right*] along with the subsequent N-terminal region residues were docked in the core ATPase structure. (*C*) Working model of bidirectional autoregulation of Rhp26 by flanking regions. Rhp26 can exhibit either a locked inactive state (with weak ATPase and no chromatin remodeling) or a super active site (with high ATPase and chromatin-remodeling activities). The N-terminal region, core ATPase domain, and C-terminal region of Rhp26 are shown in cyan, green and orange, respectively. DNA is shown in magenta.

relative DNA-affinity change of the two lobes, resulting in the translocation along the DNA and nucleosome (chromatin remodeling) (23, 24, 30). Our chemical cross-linking data suggest that the leucine latch motif is likely to dock at a specific area at lobe 2/HD2 of Rhp26. This specific interaction locks lobe 1 and lobe 2 in one conformation state and blocks the rotation of lobe 2 relative to lobe 1 during ATP-dependent translocation. This result provides a mechanistic explanation of all of the observed biochemical characteristics of the N-locked inactive state (Rhp26ΔC): low ATPase activity, no detectable chromatin-remodeling activity, and high nucleosome binding affinity. Our results also provide a mechanistic explanation for a similar N-terminal inhibitory effect observed in human CSB (20).

Bidirectional Regulation of Rhp26 by Flanking Regions Is Important for Its in Vitro and in Vivo Function. Here, we reveal that the N- and C-terminal regions of Rhp26 have opposing roles in regulating Rhp26 activity. Rhp26ΔN has the highest ATPase and chromatin-remodeling activities among all Rhp26 proteins containing the core ATPase domain (termed the superactive state). In sharp contrast, Rhp26ΔC has the lowest ATPase and no detectable chromatin-remodeling activities (termed the inactive locked state). The enzymatic activities of $Rhp26^{wt}$ are determined by a net sum of opposite contributions from both Rhp26-N and Rhp26-C.

To further elucidate this bidirectional regulatory mechanism in controlling Rhp26 activity, we propose a new working model (Fig. 5*C*) in which the N-terminal region promotes an inactive locked state (as seen with Rhp26ΔC) and the C-terminal region promotes a superactive state (as seen with Rhp26ΔN) in comparison with basal level activity contribution from the core ATPase domain of Rhp26 (Rhp26-M). In the inactive locked state, the N-terminal region enhances nucleosomal DNA binding by locking its leucine latch motif with the core domain. In this state, the conformational change of two lobes during cycles of ATP hydrolysis and ATP-dependent DNA translocation is hindered. In sharp contrast, in the superactive state, the leucine latch motif is released from the core domain to unlock the restraint between two lobes, allowing cycles of ATP hydrolysis and ATP-dependent DNA translocation. The C-terminal region of Rhp26 partially counteracts the N-terminal region function by either promoting the release of the locked N-terminal domain, greatly enhancing ATP binding/hydrolysis, or promoting conformational changes during ATP-dependent DNA translocation, and consequently enhances ATPase activity and chromatin-remodeling activity. We propose that Rhp26 can switch between these two states during translocation along the dsDNA. Our model may also apply to all ERCC6 subfamily and other homologous motor proteins.

Our studies further reveal that this bidirectional regulation by flanking regions is finely balanced in vivo because misregulation in either direction leads to toxic effects or sensitivity to DNA lesions. Overexpression of wild-type Rhp26 results in cellular toxicity. This toxicity is greatly enhanced by overexpression of the superactive forms (Rhp26ΔN, Rhp26L7G/L10G, and Rhp26L7P/L10P), which may be due to the disruption of normal chromatin structures or the depletion of ATP pools. On the other hand, cells expressing Rhp26 mutants with decreased enzymatic activity (such as Rhp26ΔC) result in DNA damage sensitivity. Taken together, our studies provide novel mechanistic insights into understanding autoregulation of Rhp26 activities and their contributions to DNA damage repair and chromatin stability maintenance in vivo.

An Emerging Theme of Flanking Regions in Regulating ATP-Dependent Chromatin-Remodeling Motors. Although the autoregulatory mechanism of Rhp26 by the leucine latch motif reported in this study is significantly different from previously reported regulatory motifs for other ATP-dependent chromatin-remodeling motors, regulation by flanking regions seems to be an emerging theme for many chromatin remodelers. For example, ISWI, a distant SNF2-like family chromatin-remodeling factor, has two ISWI-specific autoinhibitory motifs (AutoN and NegC) that negatively regulate ATP hydrolysis and the coupling ATPase with DNA translocation (2). Chd1, another distantly related SNF2-like family member, contains a Chd1-specific inhibitory chromodomain, which gated the interaction between ATPase motor and duplex DNA (3). In some members of the SNF2-like family of ATPase, N-terminal regions could also play positive regulatory roles, such as Ino80 (ATPase subunit in the INO80 chromatin-remodeling complex) and Sth1 (ATPase component of the RSC chromatin-remodeling complex) (6, 7). The variety in the details of regulatory mechanisms by flanking regions may stem from the diverse functions and specificities of these different chromatin remodelers.

Finally, our study also reveals a striking mechanistic similarity in terms of the autoinhibition of enzymatic activities of key transcription coupled repair factors in prokaryotes and eukaryotes. Prokaryotic transcription repair-coupled factor (TRCF, or Mfd) has a similar function in prokaryotic transcription-coupled repair to that of CSB albeit via a different mechanism. Intriguingly, TRCF (Mfd) also has autoinhibitory N-terminal domains that clamp with the core ATPase domain to inhibit ATPase activity via restricting the rotation of two ATPase lobes (31) although the details of interaction for TRCF are different

from that for Rhp26$^{ERCC6/CSB}$. Autoinhibition is subsequently released upon recruitment to a damage stalled transcription complex to initiate transcription-coupled repair. This parallel theme suggests that very similar regulatory strategies are used in controlling transcription-coupled repair in both prokaryotes and eukaryotes.

Conclusion

Our work provides several novel insights and conceptual advances in understanding the regulatory mechanism of ERCC6 subfamily proteins. We reveal that the molecular mechanism of the N terminus inhibitory effect is due to specific interaction between a novel leucine latch motif and the core ATPase domain, which consequently locks Rhp26 in one conformation state and blocks the rotation of lobe 2 relative to lobe 1 during ATP-dependent translocation. This evolutionarily conserved leucine latch motif is responsible for the N terminus inhibitory effect on ERCC6 enzymatic activities. Moreover, our studies also reveal that the C terminus plays an opposite regulatory role in comparison with the N terminus. Finally, we propose the concept that a fine balance between positive and negative regulations for Rhp26 is not only important for tuning Rhp26 activities, but also crucial for maintaining genome integrity and preventing cellular toxicity.

Materials and Methods

A detailed description regarding the preparation of Rhp26 and its truncations and mutants, ATPase assay, chromatin-remodeling assay, general *S. pombe* methods, and chemical cross-linking and mass spectrometry analysis can be found in *SI Materials and Methods*. Briefly, ATPase assays were carried out by incubating purified Rhp26 proteins with dsDNA in the reaction buffer containing α-[^{32}P]-ATP (Perkin-Elmer). The products were separated by microcrystalline cellulose TLC as described (32). In a mononucleosome-remodeling assay, Rhp26 proteins were incubated with reconstituted a mononucleosomal substrate, which contains a laterally positioned "601" nucleosome positioning sequence as described (33, 34). The reaction products were subjected to 5% polyacrylamide gels. Restriction enzyme accessibility assays were performed as described previously (35). *S. pombe* strains were generated and manipulated using established techniques (36). Strains and plasmids used are listed in Table S1. In the chemical cross-linking and mass spectrometry analysis, Rhp26ΔC was cross-linked with BS3 [Bis(sulfosuccinimidyl) suberate]. The reaction sample was resolved on a 4–12% Bis-Tris NuPage protein gel. The gel band corresponding to the cross-linked monomer was analyzed by trypsin digestion (37) and mass spectrometry.

ACKNOWLEDGMENTS. We thank Akira Yasui for the *S. pombe* strain that was used to derive ones used in this study. D.W. acknowledges National Institutes of Health (NIH) Grants GM085136 and GM102362 and a Kimmel Scholar Award from the Sidney Kimmel Foundation for Cancer Research. P.R. acknowledges NIH Grants GM059447, CA077325, CA117638, and P42ES010337. R.C.C. and J.W.C. acknowledge NIH Grant GM41628. J.A.R. acknowledges NIH Grants 2P50 GM076547 and R21CA175849. J.T.K. acknowledges NIH Grant GM058272.

1. Narlikar GJ, Sundaramoorthy R, Owen-Hughes T (2013) Mechanisms and functions of ATP-dependent chromatin-remodeling enzymes. *Cell* 154(3):490–503.
2. Clapier CR, Cairns BR (2012) Regulation of ISWI involves inhibitory modules antagonized by nucleosomal epitopes. *Nature* 492(7428):280–284.
3. Hauk G, McKnight JN, Nodelman IM, Bowman GD (2010) The chromodomains of the Chd1 chromatin remodeler regulate DNA access to the ATPase motor. *Mol Cell* 39(5): 711–723.
4. Alexiadis V, Lusser A, Kadonaga JT (2004) A conserved N-terminal motif in Rad54 is important for chromatin remodeling and homologous strand pairing. *J Biol Chem* 279(26):27824–27829.
5. Sigurdsson S, Van Komen S, Petukhova G, Sung P (2002) Homologous DNA pairing by human recombination factors Rad51 and Rad54. *J Biol Chem* 277(45):42790–42794.
6. Shen X, Ranallo R, Choi E, Wu C (2003) Involvement of actin-related proteins in ATP-dependent chromatin remodeling. *Mol Cell* 12(1):147–155.
7. Szerlong H, et al. (2008) The HSA domain binds nuclear actin-related proteins to regulate chromatin-remodeling ATPases. *Nat Struct Mol Biol* 15(5):469–476.
8. Flaus A, Martin DM, Barton GJ, Owen-Hughes T (2006) Identification of multiple distinct Snf2 subfamilies with conserved structural motifs. *Nucleic Acids Res* 34(10): 2887–2905.
9. Sarker AH, et al. (2005) Recognition of RNA polymerase II and transcription bubbles by XPG, CSB, and TFIIH: Insights for transcription-coupled repair and Cockayne Syndrome. *Mol Cell* 20(2):187–198.
10. Hanawalt PC, Spivak G (2008) Transcription-coupled DNA repair: Two decades of progress and surprises. *Nat Rev Mol Cell Biol* 9(12):958–970.
11. Lagerwerf S, Vrouwe MG, Overmeer RM, Fousteri MI, Mullenders LH (2011) DNA damage response and transcription. *DNA Repair (Amst)* 10(7):743–750.
12. Fousteri M, Mullenders LH (2008) Transcription-coupled nucleotide excision repair in mammalian cells: Molecular mechanisms and biological effects. *Cell Res* 18(1):73–84.
13. Troelstra C, et al. (1992) ERCC6, a member of a subfamily of putative helicases, is involved in Cockayne's syndrome and preferential repair of active genes. *Cell* 71(6): 939–953.
14. Troelstra C, Hesen W, Bootsma D, Hoeijmakers JH (1993) Structure and expression of the excision repair gene ERCC6, involved in the human disorder Cockayne's syndrome group B. *Nucleic Acids Res* 21(3):419–426.
15. van den Boom V, et al. (2004) DNA damage stabilizes interaction of CSB with the transcription elongation machinery. *J Cell Biol* 166(1):27–36.
16. van Gool AJ, et al. (1997) The Cockayne syndrome B protein, involved in transcription-coupled DNA repair, resides in an RNA polymerase II-containing complex. *EMBO J* 16(19):5955–5965.
17. Malik S, et al. (2010) Rad26p, a transcription-coupled repair factor, is recruited to the site of DNA lesion in an elongating RNA polymerase II-dependent manner in vivo. *Nucleic Acids Res* 38(5):1461–1477.
18. Selby CP, Sancar A (1997) Human transcription-repair coupling factor CSB/ERCC6 is a DNA-stimulated ATPase but is not a helicase and does not disrupt the ternary transcription complex of stalled RNA polymerase II. *J Biol Chem* 272(3):1885–1890.
19. Citterio E, et al. (2000) ATP-dependent chromatin remodeling by the Cockayne syndrome B DNA repair-transcription-coupling factor. *Mol Cell Biol* 20(20):7643–7653.
20. Lake RJ, Geyko A, Hemashettar G, Zhao Y, Fan HY (2010) UV-induced association of the CSB remodeling protein with chromatin requires ATP-dependent relief of N-terminal autorepression. *Mol Cell* 37(2):235–246.
21. Fousteri M, Vermeulen W, van Zeeland AA, Mullenders LH (2006) Cockayne syndrome A and B proteins differentially regulate recruitment of chromatin remodeling and repair factors to stalled RNA polymerase II in vivo. *Mol Cell* 23(4):471–482.
22. Licht CL, Stevnsner T, Bohr VA (2003) Cockayne syndrome group B cellular and biochemical functions. *Am J Hum Genet* 73(6):1217–1239.
23. Thomä NH, et al. (2005) Structure of the SWI2/SNF2 chromatin-remodeling domain of eukaryotic Rad54. *Nat Struct Mol Biol* 12(4):350–356.
24. Dürr H, Körner C, Müller M, Hickmann V, Hopfner KP (2005) X-ray structures of the Sulfolobus solfataricus SWI2/SNF2 ATPase core and its complex with DNA. *Cell* 121(3): 363–373.
25. Brosh RM, Jr, et al. (1999) The ATPase domain but not the acidic region of Cockayne syndrome group B gene product is essential for DNA repair. *Mol Biol Cell* 10(11): 3583–3594.
26. Anindya R, et al. (2010) A ubiquitin-binding domain in Cockayne syndrome B required for transcription-coupled nucleotide excision repair. *Mol Cell* 38(5):637–648.
27. Lake RJ, Fan HY (2013) Structure, function and regulation of CSB: A multi-talented gymnast. *Mech Ageing Dev* 134(5-6):202–211.
28. Yasuhira S, Morimyo M, Yasui A (1999) Transcription dependence and the roles of two excision repair pathways for UV damage in fission yeast Schizosaccharomyces pombe. *J Biol Chem* 274(38):26822–26827.
29. Kanamitsu K, Ikeda S (2011) Fission yeast homologs of human XPC and CSB, rhp41 and rhp26, are involved in transcription-coupled repair of methyl methanesulfonate-induced DNA damage. *Genes Genet Syst* 86(2):83–91.
30. Lewis R, Dürr H, Hopfner KP, Michaelis J (2008) Conformational changes of a Swi2/Snf2 ATPase during its mechano-chemical cycle. *Nucleic Acids Res* 36(6):1881–1890.
31. Murphy MN, et al. (2009) An N-terminal clamp restrains the motor domains of the bacterial transcription-repair coupling factor Mfd. *Nucleic Acids Res* 37(18): 6042–6053.
32. Fang M, et al. (2010) The ER UDPase ENTPD5 promotes protein N-glycosylation, the Warburg effect, and proliferation in the PTEN pathway. *Cell* 143(5):711–724.
33. Lowary PT, Widom J (1998) New DNA sequence rules for high affinity binding to histone octamer and sequence-directed nucleosome positioning. *J Mol Biol* 276(1): 19–42.
34. Owen-Hughes T, et al. (1999) Analysis of nucleosome disruption by ATP-driven chromatin remodeling complexes. *Methods Mol Biol* 119:319–331.
35. Alexiadis V, Kadonaga JT (2002) Strand pairing by Rad54 and Rad51 is enhanced by chromatin. *Genes Dev* 16(21):2767–2771.
36. Forsburg SL, Rhind N (2006) Basic methods for fission yeast. *Yeast* 23(3):173–183.
37. Shevchenko A, Tomas H, Havlis J, Olsen JV, Mann M (2006) In-gel digestion for mass spectrometric characterization of proteins and proteomes. *Nat Protoc* 1(6): 2856–2860.
38. Thompson JD, Gibson TJ, Plewniak F, Jeanmougin F, Higgins DG (1997) The CLUSTAL_X windows interface: Flexible strategies for multiple sequence alignment aided by quality analysis tools. *Nucleic Acids Res* 25(24):4876–4882.
39. Gouet P, Robert X, Courcelle E (2003) ESPript/ENDscript: Extracting and rendering sequence and 3D information from atomic structures of proteins. *Nucleic Acids Res* 31(13):3320–3323.

Supporting Information

Wang et al. 10.1073/pnas.1420227112

SI Materials and Methods

Expression and Purification of Rhp26 and Its Truncations and Mutants. The coding sequence of Rhp26 was amplified by PCR from *Schizosaccharomyces pombe* genomic DNA (*rhp26*$^{+}$ contains no introns) and inserted into the BamHI and NotI restriction sites of the pGEX6p-1 expression vector (GE Healthcare). The full-length Rhp26 coding sequence was used as a template for amplifying the Rhp26 truncations, which was then subcloned into the BamHI and NotI restriction sites of the pGEX6p-1 expression vector. The truncated Rhp26 constructs were as follows (amino acids in parentheses): Rhp26ΔN (206–973), Rhp26ΔC (1–851), Rhp26$^{4\text{-}851}$ (4–851), Rhp26$^{6\text{-}851}$ (6–851), Rhp26$^{10\text{-}851}$ (10–851), Rhp26$^{17\text{-}851}$ (17–851), Rhp26$^{25\text{-}851}$ (25–851), Rhp26$^{143\text{-}851}$ (143–851), Rhp26$^{168\text{-}851}$ (168–851), and Rhp26-M (206–851) or the pETDuet-1 expression vector [Rhp26-N (1–205) and Rhp26-C (797–973)]. Recombinant Rhp26 proteins were expressed in *Escherichia coli* strain Rosetta 2(DE3) (Novagen) and purified by a Glutathione Sepharose 4B column (GE Healthcare) or an Ni-NTA affinity column (Qiagen) (for the his-tagged N-terminal region and C-terminal region), Hi-Trap Heparin HP, and Superdex 200 10/300 GL columns (GE Healthcare). Site-directed mutagenesis of Rhp26 mutants Rhp26Δ*N*-K308R, Rhp26ΔC-L7G/L10G, and Rhp26ΔC-L7P/L10P was generated and purified in the same manner as for wild-type Rhp26.

DNA-Dependent ATPase Assay. ATPase assays were carried out by incubating Rhp26 or its truncations with dsDNA dsAT30 [30 nt of poly (dA:dT) DNA oligos] in the reaction buffer containing 20 mM Tris·HCl, pH 7.5, 4 mM $MgCl_2$, 40 μg/mL BSA, 1 mM DTT, 52 mM NaCl, 50 μM ATP, and 33 nM α-[^{32}P]-ATP (Perkin-Elmer) at 30 °C for different time points. The reaction was quenched by adding 1/2 volume of 0.5 M EDTA (pH 8.0) buffer. The products were separated by microcrystalline cellulose TLC and analyzed by Bio-Rad PharosFX Imager Plus as described (1).

Mononucleosome-Remodeling Assay. A DNA fragment carrying a laterally positioned "601" nucleosome positioning sequence was body-labeled by α-^{32}P-dCTP in a PCR using pGEM-3Z-601 as a template (2). The mononucleosomal substrate was reconstituted on this labeled DNA by transferring HeLa oligonucleosomes using a serial dilution method (3). Briefly, 3 μg of nucleosomes was mixed with 1 pmol of the labeled DNA in a total of 25 μL of reaction containing 1 M NaCl, 10 mM Tris·HCl (pH 8.0), 1 mM EDTA (pH 8.0), 5 mM DTT, and 0.5 mM PMSF. After an initial incubation of 30 min at 30 °C, the reaction was sequentially adjusted to 0.8, 0.6, and 0.4 mM NaCl by diluting with a dilution buffer containing 10 mM Tris·HCl (pH 8.0), 1 mM EDTA (pH 8.0), 5 mM DTT, and 0.5 mM PMSF, with 30 min incubation at 30 °C between each dilution. The final two dilutions to 0.2 and 0.1 M NaCl were made using the same dilution buffer plus 0.1% Nonidet P-40, 20% (vol/vol) glycerol, and 200 μg/mL BSA. Purified Rhp26 or truncated proteins were incubated at 30 °C with 0.5 μL of reconstituted mononucleosomal substrate in buffer containing 20 mM Hepes-NaOH (pH 7.9), 50 mM NaCl, 5 mM $MgCl_2$, 1 mM DTT, 1 mM PMSF, 100 μg/mL BSA, 5% (vol/vol) glycerol, 0.02% Nonidet P-40, 0.02% Triton X-100, and 1 mM ATP (USB/Affymetrix). After 60 min, 0.5 μg of HeLa oligonucleosomes (3) and 0.75 μg of salmon sperm DNA were added into the reaction with a 30-min incubation at 30 °C, which compete with DNA- or nucleosome-binding proteins that would alter substrate electrophoretic mobility. The reaction products were subjected to 5% polyacrylamide gels and resolved by electrophoresis at 4 °C for 4.5 h at 200 V. Gels were exposed to a storage phosphor screen and scanned with a Typhoon imaging scanner.

Chromatin Remodeling by Restriction Enzyme Accessibility Assays. Restriction enzyme accessibility assays were performed as described previously (4). Basically, chromatins were reconstituted by the gradient salt dialysis method by using *Drosophila* core histones and an ∼3-kb plasmid DNA. Then, 200 ng of chromatin were gently mixed with proteins of interest in 1× NEB cut smart buffer containing 3 mM ATP and 5 mM $MgCl_2$. Digestion of chromatin was performed by adding 15 U of HaeIII restriction enzyme (NEB) for 1 h at 27 °C. Samples were deproteinized, and DNA was purified, resolved by 0.8% agarose gel, and visualized by ethidium bromide staining.

General *S. pombe* Methods. Strains were generated and manipulated using established techniques (5). N-terminal FLAG-tagged *rhp26* constructs were either integrated at the genomic locus under the native promoter or cloned into pREP41 plasmids and transformed into indicated genetic backgrounds. Strains were grown in rich media (YES) or minimal media (EMM) supplemented with the appropriate amino acids. Transformed cells were grown to log-phase in the presence (repressed) or absence of thiamine (overexpressed) and subsequently plated as fivefold serial dilutions. Cells were grown in the absence of thiamine for 24 h before plating to ensure full expression. Strains and plasmids used are listed in Table S1.

Chemical Cross-Linking and Mass Spectrometry Analysis. Twenty micrograms of Rhp26ΔC was cross-linked with 0.5 mM BS3 [Bis (sulfosuccinimidyl) suberate]; Thermo Scientific) for 30 min at room temperature. The reaction was quenched by adding 2 μL of 1 M ammonium bicarbonate for 30 min at room temperature. The sample was then reduced by adding TCEP (Pierce) to a final concentration of 5 mM and incubating at 37 °C for 30 min. The sample was alkylated by adding iodoacetamide (Sigma) to a final concentration of 10 mM and incubating at room temperature for 30 min. The sample was resolved on a 4–12% Bis Tris NuPage protein gel (Life Technologies), and the gel was stained with SimplyBlue (Life Technologies). A gel band corresponding to the cross-linked monomer was excised, destained, and trypsin digested as described (6).

Trypsin digested samples were analyzed on a Thermo Scientific Orbitrap Elite with HCD fragmentation and serial MS events that included one FTMS1 event at 30,000 resolution followed by 10 FTMS2 events at 15,000 resolution. Other instrument settings included: MS mass range greater than 1,500; use *m*/*z* value as masses enabled; charge state rejection: +1, +2, and unassigned charges; monoisotopic precursor selection enabled; dynamic exclusion enabled: repeat count 1, exclusion list size 500, exclusion duration 30 s; HCD normalized collision energy 35%, isolation width 2 Da, minimum signal count 5,000; FTMS MSn AGC target 50,000. The RAW files were converted to mzXML files and analyzed by two different cross-link database searching algorithms: plink (7) and in-house designed Nexus.

A protein database containing the forward and reversed sequence of Rhp26ΔC was used for the Nexus analysis with the following parameter settings: (*i*) up to three miscleavages; (*ii*) static modification on cysteines (+57.0215 Da); (*iii*) differential oxidation modification on methionines (+15.9949 Da); (*iv*) differential modification on the peptide N-terminal glutamic

acid residues (−18.0106 Da) or N-terminal glutamine residues (−17.0265 Da); and (*v*) differential mono-BS3 modification on lysine residue (+156.0806 Da). All possible tryptic peptide pairs within 20 ppm of the precursor mass are used for cross-linked peptide searches. For each candidate peptide pair, the theoretical b- and y-ion series for each peptide is compared with the acquired spectrum with a modification mass of either the partner peptide and the BS3 linker at the cross-linking site or a cross-linker–derived lysine immonium ion plus the BS3 linker (modification mass of 221.1416 Da) at the cross-linking site. The score is calculated as the sum of the weighted dot product of the weighted candidate ion series and the normalized intensity of each fragment ion within 60 ppm of the theoretical fragment ion (similar to the normalization procedure used by the Sequest algorithm) (8). The weighted ion matrix considers both the coexistence and connectivity of fragment ions: Each candidate ion is weighted 1 at a given charge state; if the preceding ion of the same charge state is present, the score is increased by 0.5; if not, the score is decreased by 0.5; the same rules apply to the subsequent ion in the ion series. If the weight of an ion equals zero, then a minimum weight of 0.5 is given. The highest candidate score is kept for each spectrum. The false-positive rate (FDR) is calculated as the number of identifications containing one decoy sequence (U) minus the number of identifications containing two decoy sequences (F) divided by the number of identifications containing no decoy sequences (T): FDR = (U − F)/T. This result is similar to the FDR calculation used by pLink (7).

After performing the pLink and the Nexus analyses and applying a 5% FDR cutoff, the search results were combined and each spectrum was manually evaluated for the quality of the match to each peptide using the COMET/Lorikeet Spectrum Viewer (TPP). The specific intramolecular lysine residues cross-linked with the free amine group of the short N-terminal peptide containing the "Leucine-latch" motif (GPLGSMSVNEDLSHLGVFSVDQENLER) were identified by chemical cross-linking/mass spectrometry analysis (Fig. 5*A* and Fig. S7*D*). The cross-linked peptides were considered confidently identified if at least four consecutive b or y ions for each peptide were observed and the majority of the observed ions were accounted for.

1. Fang M, et al. (2010) The ER UDPase ENTPD5 promotes protein N-glycosylation, the Warburg effect, and proliferation in the PTEN pathway. *Cell* 143(5):711–724.
2. Lowary PT, Widom J (1998) New DNA sequence rules for high affinity binding to histone octamer and sequence-directed nucleosome positioning. *J Mol Biol* 276(1):19–42.
3. Owen-Hughes T, et al. (1999) Analysis of nucleosome disruption by ATP-driven chromatin remodeling complexes. *Methods Mol Biol* 119:319–331.
4. Alexiadis V, Kadonaga JT (2002) Strand pairing by Rad54 and Rad51 is enhanced by chromatin. *Genes Dev* 16(21):2767–2771.
5. Forsburg SL, Rhind N (2006) Basic methods for fission yeast. *Yeast* 23(3):173–183.
6. Shevchenko A, Tomas H, Havlis J, Olsen JV, Mann M (2006) In-gel digestion for mass spectrometric characterization of proteins and proteomes. *Nat Protoc* 1(6):2856–2860.
7. Yang B, et al. (2012) Identification of cross-linked peptides from complex samples. *Nat Methods* 9(9):904–906.
8. Eng JK, Fischer B, Grossmann J, Maccoss MJ (2008) A fast SEQUEST cross correlation algorithm. *J Proteome Res* 7(10):4598–4602.

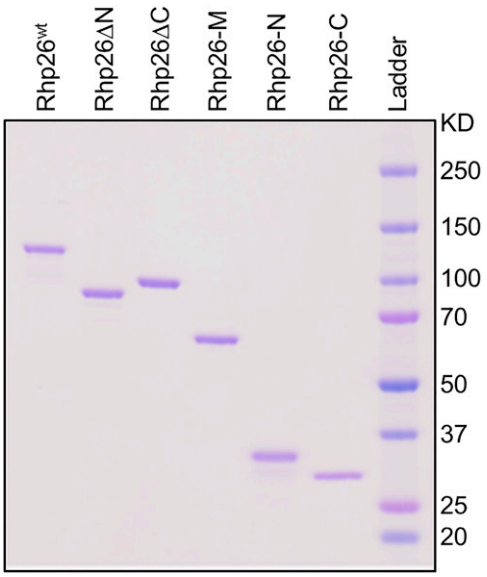

Fig. S1. Purified Rhp26 and Rhp26 truncations. Purified recombinant proteins used in this study, analyzed by SDS/PAGE stained with Coomassie blue R250. Molecular mass standards are shown at the far right.

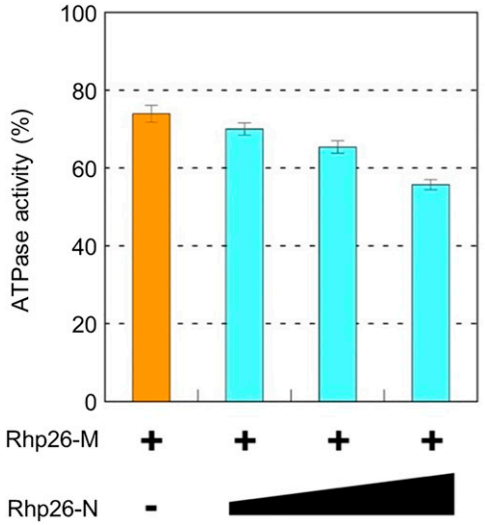

Fig. S2. Rhp26-N decreases the ATPase activity of Rhp26-M *in trans*. Rhp26-M concentration is at 250 nM, and Rhp26-N concentration increases from 0 to 1,500 nM (0, 250, 750, and 1500 nM, left to right). Error bar is the SD based on two individual experiments.

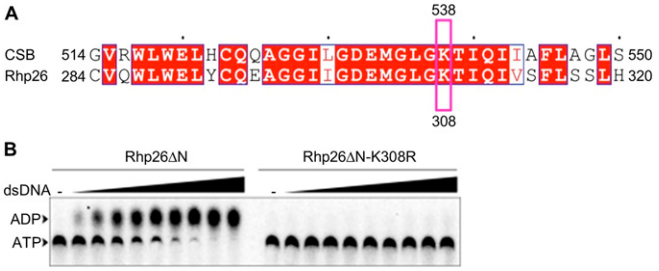

Fig. S3. The catalytically dead mutant, Rhp26Δ*N*-K308R, fully abolishes the ATPase activity of Rhp26. (*A*) Sequence alignment of key residues in motif I of CSB and Rhp26. The key lysine residue that is critical for ATPase activity is highlighted with a magenta rectangle; conserved region, blue rectangle; strictly conserved residues, red background. (*B*) The catalytically dead mutant, Rhp26Δ*N*-K308R, fully abolishes the ATPase activity of Rhp26. Protein concentration was 500 nM, the dsDNA concentration was increased from 0 to 500 nM (0, 10, 20, 30, 40, 50, 75, 100, 200, and 500 nM, left to right), and the reactions were performed at 30 °C for 1 h.

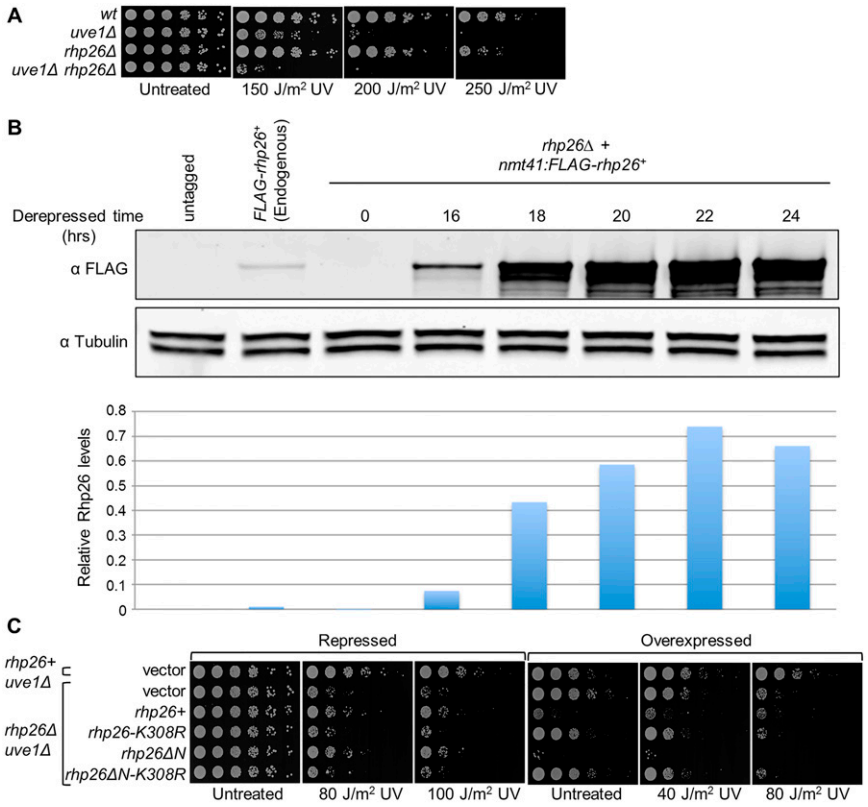

Fig. S4. Analysis of Rhp26 mutants in *S. pombe*. (*A*) Rhp26 and Uve1 (Uvde) function in parallel pathways in the repair of UV-induced DNA damage. (*B*) Expression levels of Rhp26 expressed from endogenous and nmt41 promoter. (*C*) Toxicity of *rhp26*$^{+}$ and *rhp26ΔN* overexpression is dependent on the ATPase activity of Rhp26. For all above experiments, fivefold serial dilutions of log-phase cells with the indicated genotypes were plated and exposed to the indicated dose of UV irradiation or alkylating agent methyl methanesulfonate (MMS).

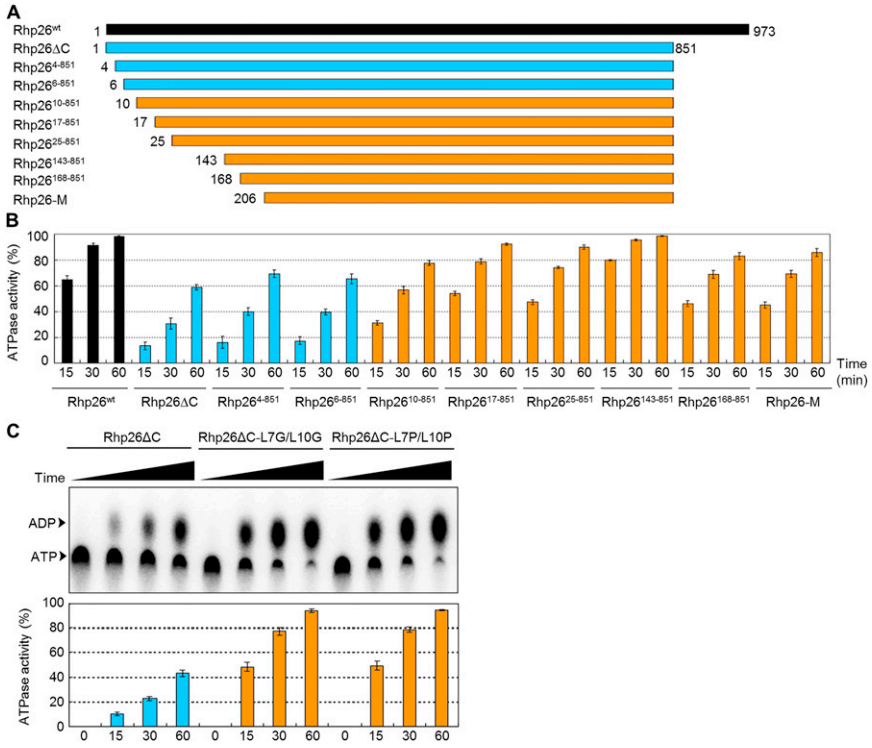

Fig. S5. Mapping the residues at the N-terminal region that are responsible for Rhp26 regulation. (*A*) Constructs of N-terminal deletion based on Rhp26ΔC. Constructs behaving similarly were shown in the same color. Black, wild-type; cyan, Rhp26ΔC and those with inhibited ATPase activity; orange, core ATPase domain and those with increasing ATPase activity compared with Rhp26ΔC. (*B*) The ATPase activity of Rhp26 truncations with different N-terminal deletions. The error bar is the SD based on three independent experiments, and the color code is the same as in *A*. (*C*) Rhp26ΔC-L7G/L10G and Rhp26ΔC-L7P/L10P mutations (orange) rescue the N-terminal region inhibition of Rhp26ΔC ATPase activity. The error bars in this figure are the SD based on three independent experiments.

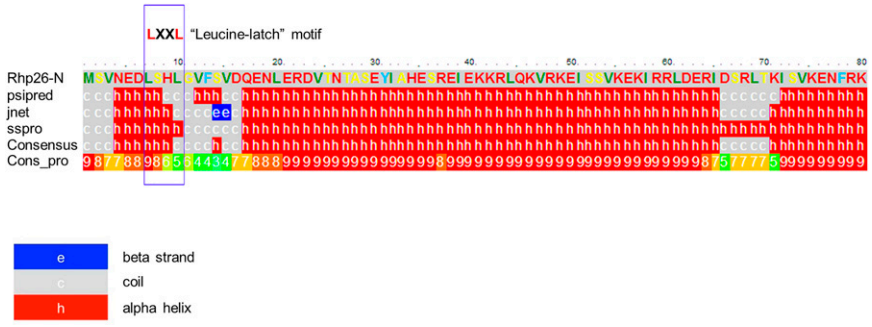

Fig. S6. The secondary structure prediction of Rhp26-N using the Phyre server (1).

1. Kelley LA, Sternberg MJ (2009) Protein structure prediction on the Web: A case study using the Phyre server. *Nat Protoc* 4(3):363–371.

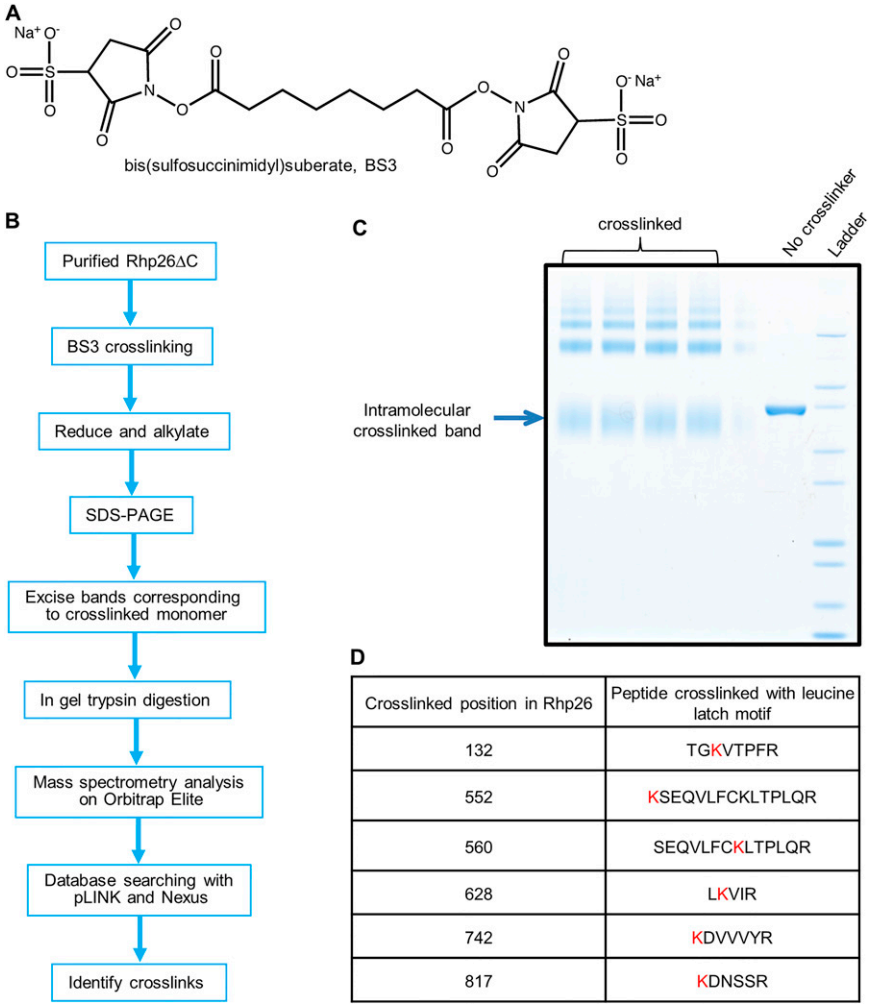

D

Crosslinked position in Rhp26	Peptide crosslinked with leucine latch motif
132	TGKVTPFR
552	KSEQVLFCKLTPLQR
560	SEQVLFCKLTPLQR
628	LKVIR
742	KDVVVYR
817	KDNSSR

Fig. S7. Chemical cross-linking and mass spectrometry analysis. (*A*) Structure of chemical cross-linker BS3. (*B*) Flowchart of chemical cross-linking/mass spectrometry analysis. (*C*) SDS gel analysis of cross-linked protein. (*D*) Specific lysine residues intramolecularly cross-linked with the free amine group of an N-terminal short peptide containing the leucine latch motif are identified by chemical cross-linking and mass spectrometry analysis.

Table S1. *S. pombe* strains and plasmids used in this study

Strain/plasmid	Genotype	Source
Strain no.		
PR109	*h- leu1-32 ura4-D18*	Lab stock
OL5190	*h- uve1::LEU2 leu1-32 ura4-D18*	This study*
OL5000	*h- rhp26::natMX6 leu1-32 ura4-D18*	This study
OL5191	*h+ rhp26::natMX6 uve1::LEU2 leu1-32 ura4-D18*	This study
OL5192	*h- 3FLAG-rhp26(1-973) leu1-32 ura4-D18*	This study
OL5193	*h- 3FLAG-rhp26(1-973)-K308R leu1-32 ura4-D18*	This study
OL5194	*h- 3FLAG-rhp26ΔC(1-851) leu1-32 ura4-D18*	This study
OL5195	*h- 3FLAG-rhp26ΔN(206-973) leu1-32 ura4-D18*	This study
OL5196	*h- 3FLAG-rhp26ΔN(206-973)-K308R leu1-32 ura4-D18*	This study
OL5197	*h- 3FLAG-rhp26-M(206-851) leu1-32 ura4-D18*	This study
OL5198	*h- 3FLAG-rhp26-N(1-205) leu1-32 ura4-D18*	This study
OL5199	*h- 3FLAG-rhp26-C(797-973) leu1-32 ura4-D18*	This study
OL5200	*h- uve1::hphMX6 leu1-32 ura4-D18 + pREP41-3FLAG*	This study
OL5201	*h- rhp26::natMX6 uve1::hphMX6 leu1-32 ura4-D18 + pREP41-3FLAG*	This study
OL5202	*h- rhp26::natMX6 uve1::hphMX6 leu1-32 ura4-D18 + pREP41-3FLAG-rhp26(1-973)*	This study
OL5203	*h- rhp26::natMX6 uve1::hphMX6 leu1-32 ura4-D18 + pREP41-3FLAG-rhp26ΔN(206-973)*	This study
OL5204	*h- rhp26::natMX6 uve1::hphMX6 leu1-32 ura4-D18 + pREP41-3FLAG-rhp26ΔC(1-851)*	This study
OL5205	*h- rhp26::natMX6 uve1::hphMX6 leu1-32 ura4-D18 + pREP41-3FLAG-rhp26-N(1-205)*	This study
OL5206	*h- rhp26::natMX6 uve1::hphMX6 leu1-32 ura4-D18 + pREP41-3FLAG-rhp26-M(206-851)*	This study
OL5207	*h- rhp26::natMX6 uve1::hphMX6 leu1-32 ura4-D18 + pREP41-3FLAG-rhp26-C(797-973)*	This study
OL5208	*h- rhp26::natMX6 uve1::hphMX6 leu1-32 ura4-D18 + pREP41-3FLAG-rhp26(1-973)-K308R*	This study
OL5209	*h- rhp26::natMX6 uve1::hphMX6 leu1-32 ura4-D18 + pREP41-3FLAG-rhp26ΔN(206-973)-K308R*	This study
Plasmid no.		
pPC554	*pREP41-3FLAG*	This study
pPC549	*pREP41-3FLAG-rhp26(1-973)*	This study
pPC550	*pREP41-3FLAG-rhp26ΔN(206-973)*	This study
pPC551	*pREP41-3FLAG-rhp26ΔC(1-851)*	This study
pPC548	*pREP41-3FLAG-rhp26-N(1-205)*	This study
pPC552	*pREP41-3FLAG-rhp26-M(206-851)*	This study
pPC547	*pREP41-3FLAG-rhp26-C(797-973)*	This study
pPC556	*pREP41-3FLAG-rhp26(1-973)-K308R*	This study
pPC564	*pREP41-3FLAG-rhp26ΔN(206-973)-K308R*	This study
pPC549	*pREP41-3FLAG-rhp26L7P/L10P*	This study
pPC549	*pREP41-3FLAG-rhp26L7G/L10G*	This study
pPC549	*pREP41-3FLAG-rhp26-L7P/L10P/K308R*	This study
pPC549	*pREP41-3FLAG-rhp26-L7G/L10G/K308R*	This study

*Derived from strain Y53 (1).

1. Yasuhira S, Morimyo M, Yasui A (1999) Transcription dependence and the roles of two excision repair pathways for UV damage in fission yeast Schizosaccharomyces pombe. *J Biol Chem* 274(38):26822–26827.